Article

Detection of Migrating and Non-Migrating Atmospheric Tides Derived from ERA5 Temperature Meteorological Analyses

Philippe Keckhut *, Thomas Lefebvre, Alain Hauchecorne [ID] **, Mustapha Meftah and Sergey Khaykin**

Laboratoire Atmosphères, Observations Spatiales (LATMOS), Institut Pierre Simon Laplace (IPSL), Université Paris-Saclay, UVSQ, Sorbonne Université, CNRS, 78280 Guyancourt, France; thomas.lefebvre@latmos.ipsl.fr (T.L.); alain.hauchecorne@latmos.ipsl.fr (A.H.); mustapha.meftah@latmos.ipsl.fr (M.M.); sergey.khaykin@latmos.ipsl.fr (S.K.)
* Correspondence: keckhut@latmos.ipsl.fr

Abstract: To better extract the tides represented in the European meteorological analysis ERA5, an analysis of the histograms of the diurnal and semi-diurnal modes as a function of longitudes was performed. This analysis revealed that modes with different characteristics appeared regionally along a single longitude. Retrieved migrating tides were compared with a tidal model showing global agreement below 60 km and twice the amplitude in meteorological analyses at mid-latitude. Non-migrating tidal modes have been identified along the tropical band. They logically appear above the convective zones, probably due to water vapor excess. Their characteristics are different from migrating components. This preliminary study has shown that it is necessary to develop additional observations allowing for more frequent sampling to retrieve migrating and non-migrating tides that can only be achieved with satellite constellations from space.

Keywords: temperature; atmosphere; tides; space; cubesat; mesosphere

1. Introduction

Atmospheric tides are caused by solar radiation on the diurnal cycle, by water vapor, and by ozone. As a consequence, temperature and wind are modified due to the absorption of radiation. The composition of the atmosphere (and in particular ozone) is also modified by photo-dissociation. This well-known mechanism, called migrating tides, generates inertia–gravity waves of diurnal and semi-diurnal periods that propagate in the atmosphere synchronized with the rotation of Earth (synchronized with the sun). The basic characteristics of atmospheric tides are described by classical tidal theory. Ideally, tidal theory shows that tides correspond to atmospheric waves that can be viewed as linear perturbations of a zonal, horizontally stratified, isothermal mean state. In fact, atmospheric tides are natural modes of the atmosphere that can be mathematically described by Hough functions having amplitudes increasing exponentially with altitude [1]. While the atmospheric structure is not fully zonally uniform and has daily, monthly, and decadal fluctuations, tide characteristics can be different from theory [2].

Quantifying these fluctuations is a difficult challenge, as frequent observations are needed to sample diurnal cycles. Information about atmospheric tides has been possible through continuous observations over the same site by meteorite radars for wind [3,4] and temperature [5] in the upper mesosphere and lower thermosphere or by lidar for temperature in the middle atmosphere [6–9] and lower thermosphere [10]. Fluctuations in water vapor and ozone through photo-dissociation have also been observed with microwave instruments [11,12]. Atmospheric tides have also been assessed on a global scale from orbiting satellites, either by their twice-daily passes in assuming certain characteristics of the tides (notably their phases), or from instruments that do not have a synchronous orbit with the sun, such as UARS [13,14] or SABER/TIMED [15]. In this case, successive shifts each day giving different measurement times over the same location cover the whole

diurnal cycle in 60 days. However, the large diurnal variability induces spectral aliasing effects especially with planetary waves when the atmosphere is under-sampled. Conversely, quantification of tidal characteristics are biased at mid and high latitudes [16].

Information on tidal characteristics is crucial when comparing measurements that were not made at the same time and, even more, to estimate decadal trends [17] in the middle atmosphere when the orbits of successive satellites have changed [16] or when orbits drift with time [18]. Similar problems arise when data are assimilated to produce re-analyses, if the tidal modeling is not sufficiently realistic and if the tidal characteristics themselves evolve or are modified by background fields due to climate change [2]. Specific global modeling of migrating tides [19] assumes a zonally homogeneous steady atmosphere. Developments associated with the global atmospheric tide model [20] have shown good overall agreement with observations with, however, smaller amplitudes with models compared to observations [21] at mid latitudes. Comparisons with European meteorological analyses, assimilating radiosondes, and operational satellites show semi-diurnal fluctuations consistent with ECMWF (European Centre for Medium-Range Weather Forecasts) with theoretical estimates given by the GSWM model. However, the observed diurnal fluctuations reveal significant geographical differences and sometimes different characteristics of tides, probably due to ground and tropospheric effects.

A clearer understanding of tidal changes will be useful for improving methodologies in trend estimates, data assimilation, and local radiative issues. The separation of both types of tides is not trivial; however, the global/regional nature of their extension is proposed to identify both tidal components included in meteorological/climate models that provide global and continuous coverage. Observations are missing for such analyses. To better provide direct information on temperature tides, a constellation of small satellites has been suggested [22], while long-term observations from space clearly show difficulties in providing continuity using successive sensors [17,18]. However, the location and nature of all type of tides will help in defining characteristics of the required constellation.

Initial global modeling generally involves migrating tides [19] and assumes a zonally homogeneous atmosphere. Developments associated with the global atmospheric tidal model [20] have shown good overall agreement with observations with, however, lower modeled amplitudes compared to observations [21], which is probably due to intermittency effects as observed in continuous airglow [23]. Comparisons with European meteorological analyses assimilating radiosondes and operational satellites to the upper stratosphere show semi-diurnal fluctuations consistent between ECMWF (European Centre for Medium-Range Weather Forecasts) and theoretical estimates given by the Global-Scale Wave Model (GSWM) described in Section 2.2. However, the observed diurnal fluctuations reveal significant geographical differences and, sometimes, different characteristics of migrating tides, probably due to ground and tropospheric effects.

If the atmospheric fields for composition and dynamical parameters show large variability, tidal characteristics may vary [2], and non-migratory components may appear. Migrating tides propagate westward in longitude synchronously with the rotation of the sun (sun-synchronous), while non-migrating tides can propagate either westward or eastward, or be stationary and lie in a regional zone. In the latter case, the tides do not propagate with the rotation of the sun but according to the passage of the sun. They should be generated by a zonal asymmetric thermal forcing induced by large longitudinal variations in tropospheric humidity and have been observed in the lower stratosphere using GPS radio occultation observations from space [24]. The meteorological analyses have been extended to the mesopause (80 km) with a larger data set (ERA5), allowing for the study and update of tidal characteristics and the specific contribution of non-migrating tides. To better provide direct information on temperature tides, a constellation of small satellites has been suggested [22], while long-term observations from space clearly show difficulties in providing continuity using successive sensors [17,18].

In this study, we propose to investigate meteorological analyses (ERA5) to extract migrating and non-migrating tides in the middle atmosphere while analyses are performed

up to the mesopause. In Section 2, data are presented. The methodology to extract local tides is described in Section 3, as well as the separation of migrating and non-migrating modes. In Section 4, migrating tidal amplitudes and phases are compared with the Global Scale Wave Model (GSWM), while Section 5 presents non-migrating components. Section 6 discusses the results and their impact on observation requirements. Section 7 provides conclusions.

2. Description of the Data

2.1. Description of ERA5 Re-Analyses

The ERA5 numerical model is a weather and climate model [25] developed by the Copernicus Climate Change Service of the European Centre for Medium-Range Weather Forecasts (ECMWF). ERA5 is a reanalysis dataset combining various observations (ground, weather balloon, satellite) and a mathematical model constructed around primitive dynamic equations [26] governing atmospheric motions with equations of moist processes and convection, ground interactions, and physico-chemistry equations. The model is therefore constantly adjusted according to the arrival of observations. This method makes it possible to best approach the reality of the phenomena and to make forecasts [27]. This model simulates many atmospheric, oceanic, and terrestrial variables, including dynamic parameters (pressure, temperature, wind) and density of atmospheric species, including radiatively active ones for tides like ozone, water vapor, and oxygen. In addition to providing global forecasts, these analyses are carried out regularly over a long period with the same model in order to monitor changes, particularly in relation to anthropogenic forcing.

Here we use the latest version, named ERA5 [28]. Data series extend from 1950 to today and present a temporal resolution of one hour with a horizontal resolution of $2.5°$, corresponding to 144 longitudes and 73 latitudes. Vertically, the data extend from the surface up to 0.01 hPa (about 80 km altitude). Vertically, the model is divided into 137 levels, each defined by a level of pressure. In order to develop the methodology, the data used here cover a full week from 24 January to 31 January 2021 (i.e., 192 h). This length was chosen to hold the mean temperature relatively constant, expecting stationary tides (Figure 1). Therefore, 29 levels are used, from 31 to 80 km in altitude. A short period was used to develop the methodology rather than to fully evaluate the model or the seasonality of tide characteristics. The winter period was selected because most of the tide information was retrieved through lidar observation over the northern hemisphere during the time when night is the longest [6,7,9,21].
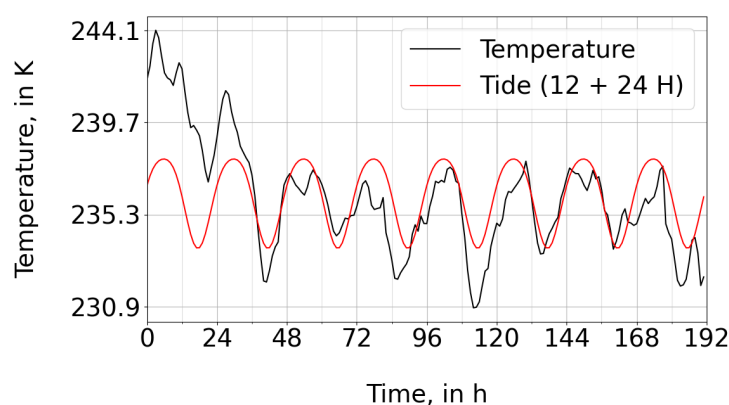
Figure 1. Temperature evolution provided by ERA5 meteorological analyses extrapolated for the altitude of 57 km above the location 5° N, 213° E. The red curve corresponds to a fit with a combination of a daily and semi-daily oscillations.

2.2. Description of the GSWM Model

The Global Scale Wave Model (GSWM) [20] is a two-dimensional linear model proposing a simulation of the migrating tides. It simulates the theoretical evolution of five atmospheric variables over time: wind, temperature, pressure, density, and the average

background level of ozone. In addition to this, it simulates photo-chemical forcing in the atmosphere, including the absorption of solar radiation. This model assumes perfect longitudinal homogeneity of the variables considered. The GSWM solves the Navier–Stoke equations for steady-state global temperature and wind perturbations. The model provides improved tide results from the initial theory in using updated data like background climatologies of temperature, wind, ozone, and wave dissipation. The result of the simulations provides monthly data extending from 0 to 125 km in altitude (31 levels) and going from one pole to the other (87° S–87° N) in steps of 3°. For each of the 5 variables, we find the amplitude and the phase at the origin of the sinusoidal functions of 12 and 24 h describing the evolution of the parameter according to time at a given point.

3. Temperature Tide Identification

3.1. Calculation of Tidal Characteristics

All the disturbances induced by dynamic parameters can propagate in the whole atmosphere. Diurnal signals (24 h) induced by tidal forcing can be detected everywhere, in addition to harmonics, with the former exhibiting a period of 12 h. In practice, strong interactions occur between planetary waves and tides up to the thermopshere [29].

To extract both components of the atmospheric tides from temperature series, data are fitted using a combination of 12- and 24-h oscillations. Tidal anomalies as a function of time (t) can be represented by the following formula as defined in the climatological model [20]:

$$\Delta T(t) = \alpha_{12} \cos\left[2\pi.f_{12}.t + \phi_{12}\right] + \alpha_{24} \cos\left[2\pi.f_{24}.t + \phi_{24}\right] \tag{1}$$

with α_i being, respectively, semi-diurnal and diurnal amplitudes expressed in Kelvin. The time (t) is given in hours, with the frequency f_i being in 1/h. ϕ_i is the phase given in radians, and the ratio between the time of maximum (in hours) and f_i, the frequency of tidal oscillations, is also expressed in 1/h. The respective values for the semi-diurnal and diurnal components as well as their respective phases (time of maximum) vary at each grid point. Two weeks have been used as a good compromise to improve the signal-to-noise ratio and keep a relatively low uncertainty. In the example presented in Figure 1, the diurnal mode dominates, and amplitudes of the tides vary slightly with time while the mean temperature varies, complicating calculations of tide estimates.

3.2. Tide Histograms

Concerning migrating modes, tidal characteristics are supposed to be similar along a single latitude. Due to the random error associated with the time of maximum (phase), histograms of tidal anomalies show a Gaussian-type shape allowing us to extract estimates of the mean value and an associated uncertainty of the phase. In the example shown in Figure 2 top, time of maximum for diurnal migrating tides is, as expected, around 18 h, with an uncertainty of ±2 h. However, in many other cases, histograms exhibit multi-modal distributions (see Figure 2 middle and bottom) with main and secondary modes that are possibly associated with non-migrating tides located at some specific locations or simply due to uncertainties in deriving tidal characteristics when amplitudes are small. Each maximum of the distribution has been fitted with Gaussian envelopes, allowing us to derive for each latitude one or two tidal phases and amplitudes as well as uncertainties depending on the width of the individual Gaussian.

The method used is called KDE (kernel density estimation). This method, also called the Parzen–Rosenblatt method [30], makes it possible to estimate the probability density of a variable. It is based on a sample population and estimates the population density at all sample points. This method is frequently used to generalize an estimation by histogram. The KDE is defined by two parameters, the kernel (K) and the window (h), according to the formula of the density probability given below:

$$d_h(x) = \frac{1}{N.h}\sum_{i=1}^{N} K\frac{(x - x_i)}{h}. \tag{2}$$

We are looking for Gaussian (normally distributed) modal distributions, and a Gaussian kernel with the following form is retrieved:

$$K = \frac{1}{\sqrt{2\pi}} \exp^{\left(-\frac{1}{2}x^2\right)}. \tag{3}$$

To avoid the hassle of setting the fit, an alternative method was used. This is called the Gaussian mixture model [31]. It makes it possible to model several Gaussian modes and to extract the weight of each mode in the distribution, its mathematical expectation, and its variance. Both methods give similar results. However, because the number of iterations is the only parameter required to be fixed, the second method was better adapted for implementation in the analysis of a large data set. An example of the fit is represented in Figure 2. Histograms reveal that, several diurnal or semi-diurnal tidal components can be observed.
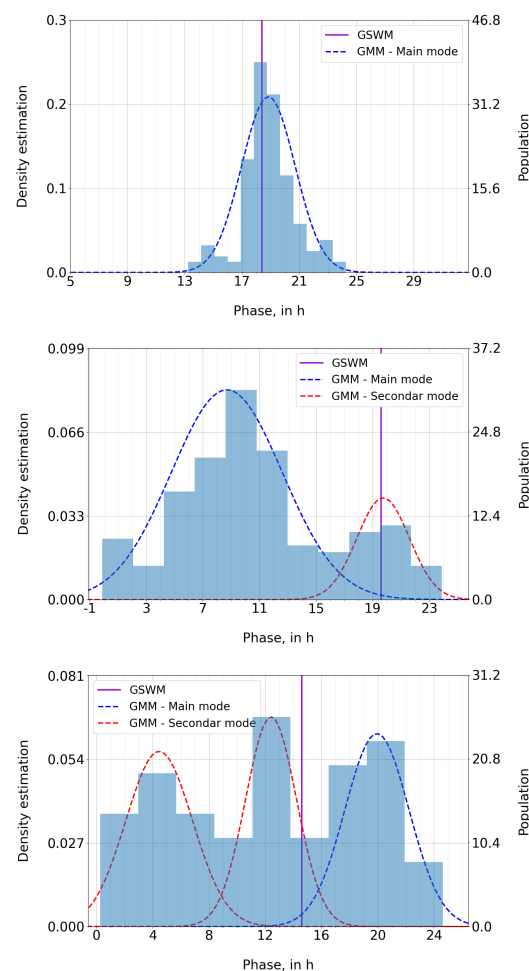

Figure 2. Some examples of histograms for the distribution of diurnal tidal temperature anomalies from ERA5 meteorological analyses over all longitude grid points for three different cases. Distributions are expressed in density probability and the number of longitude (population) steps over the 144 beams. Sampling the full longitudes: (**Top**), at 32 km in altitude on the latitudinal band around 10° N; (**Middle**), at 66 km in altitude on the latitudinal band around 60° N; (**Bottom**), at 64 in km altitude on the latitudinal band around 80° N.

4. Comparisons of Tidal Characteristics with Theory

While several modes can be observed for a single latitude (Figure 2), it is not always obvious how to identify the values corresponding to migrating modes as expected from theory (as provided by the GSWM model). The closest values are selected as the migrating

mode in spite of the fact that sometimes it does not correspond to the strongest mode. However, good agreements can be reported between the tides retrieved from ERA5 analyses using the methodology described in Section 3.2 and the GSMW [20] monthly mean tidal characteristics. Comparisons of the phases show good agreements within error bars for both modes and for low and higher latitudes in the altitude range up to 60 km. Above this altitude, times of maximum differ and are out of phase by half a period (Figures 3 and 4). Over the equator, tidal amplitudes are similar to the GSWM with, however, different vertical behavior (Figure 3 top) around 50 km for the semi-diurnal mode and above 60 km for the diurnal mode. At mid-latitude (Figure 4 top), results similar to past analyses show amplitudes nearly half [21] the expected ones up to 60 km, showing larger observed amplitudes than expected. Phases are in good agreement between observations and simulations with some drifts with altitude probably associated with the damping of the variability in the mesosphere [32].

Tidal amplitudes as a function of latitude and altitude correspond to the well-known butterfly-wing distribution (Figure 5). A different behavior is obtained at the equator with a maximum around the stratopause and around the equatorial zone in a $\pm 15°$ band. From this figure, conclusions similar to the ones associated with the vertical profiles above the equator (Figures 3 and 4) can be drawn. Larger amplitudes than the ones predicted by the model are extracted from the ERA5 series. Above 60 km, retrieved responses appear to be more inconsistent. Differences can be also observed for phases between mid-latitude and the equator. Amplitudes for the semi-diurnal mode are similar in magnitude, but the retrieved space pattern exhibits more noise (Figure 6). Also, the large increase in amplitude simulated at the equatorial latitude above 60 km reported by GSWM (Figure 5) is not captured by ERA5.
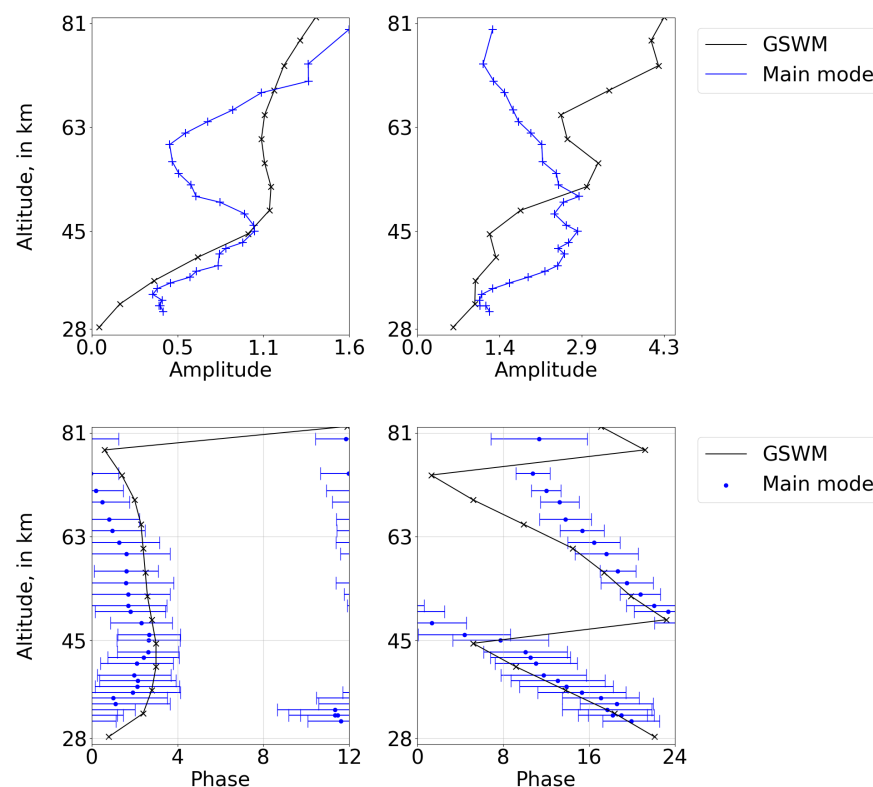
Figure 3. Vertical profiles of amplitudes expressed in temperature (**top**) and phases expressed in hours (**bottom**) of the semi-diurnal (**left**) and diurnal (**right**) tides extracted from ERA5 meteorological analyses at the equator (blue lines) compared with the characteristics given by the GSWM (black lines). Horizontal bars for the phase estimates correspond to the uncertainties.
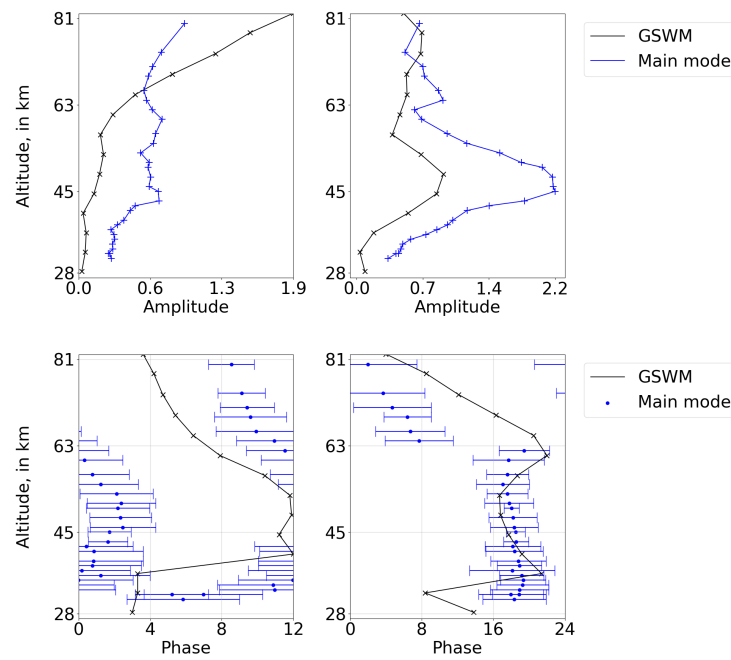
Figure 4. See caption for Figure 3, here applied for the latitude band of 45° N (blue lines).
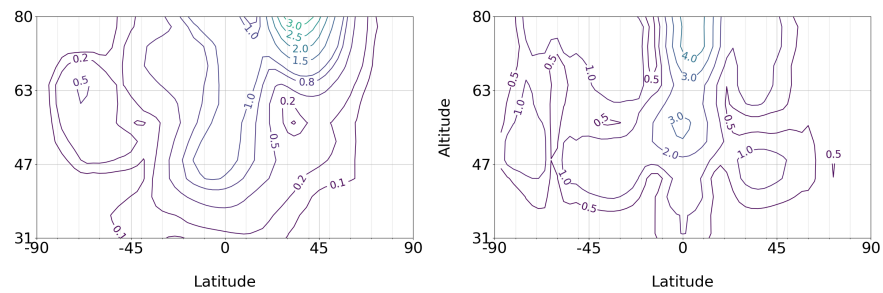

Figure 5. Phases of the diurnal tides (time of the maximum) in hours as a function of altitude and latitude deduced from ERA5 meteorological analyses (**right**) and from the GSWM (**left**) [20].
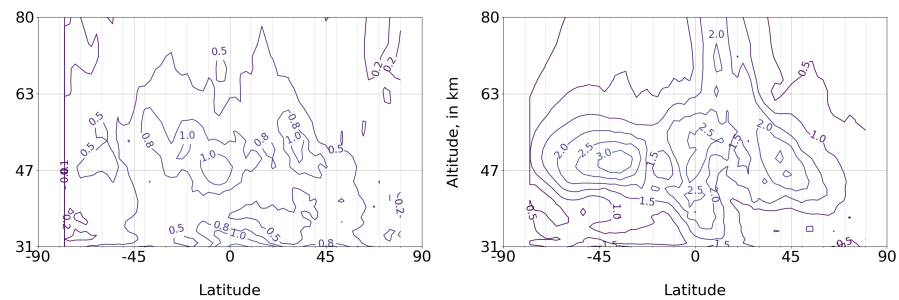

Figure 6. See caption for Figure 5, here applied for semi-diurnal tides.
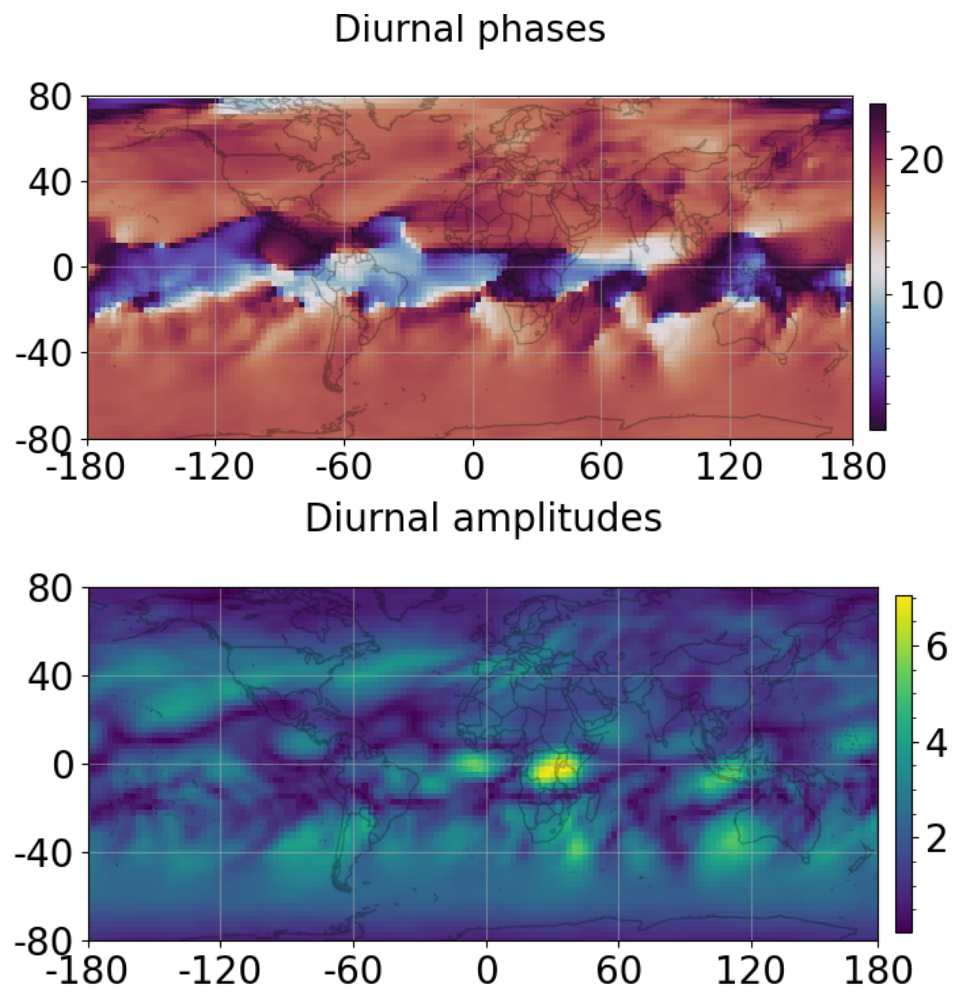
5. Non-Migrating Tides

While we expect from theory quasi-uniform characteristics in longitude for migrating tides, local retrievals show several areas where it is not true (Figure 7), thanks to the histogram approach. In the northern hemisphere, we note that the eastern part is exhibiting fluctuations over several hours (Figure 6, top), while the western part shows large phase differences for the amplitudes (Figure 7, bottom). In the southern hemisphere, phases are more uniform. However, in the tropical belt, larger differences (around 12 h) can be observed at some locations collocated with larger amplitudes. Different phases can be

observed mainly above Central America, equatorial Africa, and Indonesia (Figure 6, top). Similarly, tidal amplitudes are larger in the north of South America, equatorial Africa, the southern Indian Ocean, and Indonesia. These areas are well-known for having an intense convective zone and high water vapor content, inducing additional local radiative effects [33–35]. The border between the equatorial zone and the subtropical zone is quite disturbed, and tides exhibit complex behaviors that are difficult to interpret, probably because of the interactions between tides with other dynamic features.

To be able to extract non-migrating tides, the analysis was based on the temperature series with the migrating tide evolution removed, calculated using the main mode assumed to be related to migrating modes, and observed on the histogram (see Section 3.2). After removing the migrating component, the remaining sun-synchronous anomalies should correspond to the non-migrating modes as observed in Figure 8. As expected, zones with maximum amplitudes are similar, with the largest anomalies presented in Figure 7. Vertical profiles of tidal characteristics have been retrieved for two different zones (Figure 9) showing the largest amplitudes of the non-migrating tides (as seen in Figure 8). The first zone is located around the Indian Ocean, where tidal amplitudes present a maximum around the stratopause (Figure 10) similarly to the non-migrating mode (Figure 3 Top). While the amplitude of the semi-diurnal mode is similar to the migrating mode, the diurnal mode exhibits a larger amplitude by 1 Kelvin. over the whole vertical range from 30 to 80 km. In the mesosphere, amplitudes and phases of the semi-diurnal mode are not reported here because uncertainties in phase estimates were too large to be significantly considered. In the stratosphere, according to the migrating component (Figure 3 bottom), the retrieved phases of the tides are different by 4 h and 12 h, respectively, for the semi-diurnal and diurnal modes. Times of maximum (phases) decrease with altitude corresponding to an upward vertical propagation with a vertical speed similar to the migrating component (see Figure 3).

The analysis of the second zone, corresponding to tropical Africa (Figure 11), shows results similar to the preceding zone for amplitudes. Phases are also similar up to 35 km. For altitudes above 35 km, characteristics are slightly different than the other zone and much more similar to the migrating mode derived in Figure 3. While the origin of the non-migrating tides was clearly associated with convective latent heat release in the troposphere, the thermal response is not well-known. Some studies suggest that the contribution of gravity waves above convective systems [36] and overshooting updrafts [37] are responsible for these local diurnal temperature changes. These thermal effects involve small-scale processes and are probably not fully represented in meteorological models used to produced ERA5 analyses. However, thermal changes are probably forced in these meteorological analyses through the assimilation of radiosondes and GPS-RO observations in the troposphere and lower stratosphere [24].
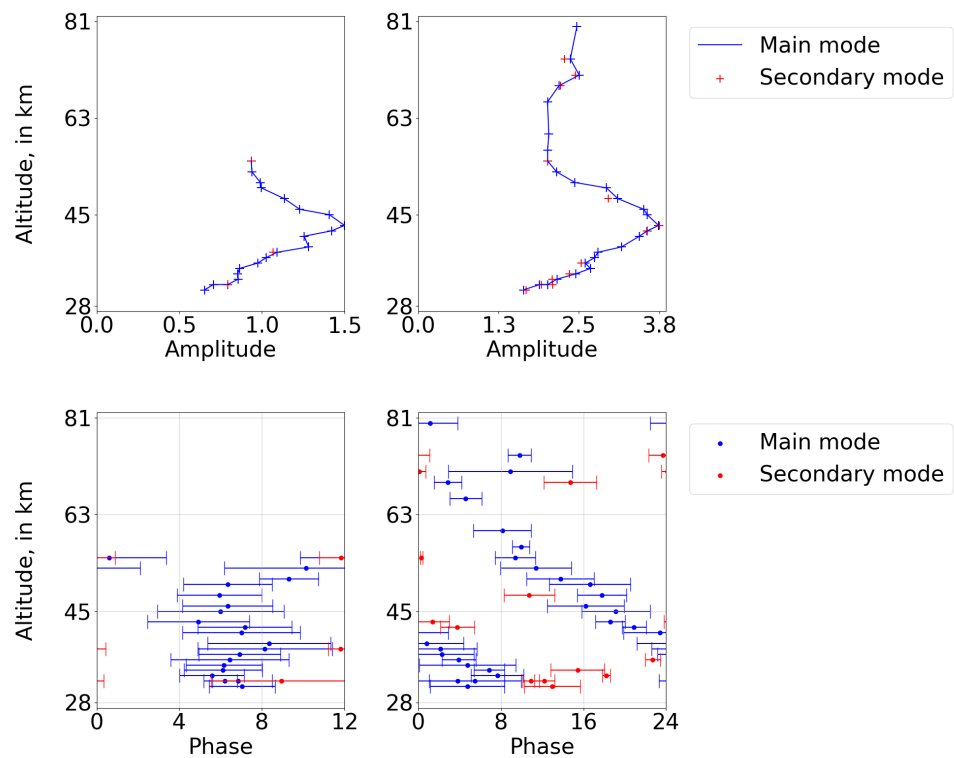
Diurnal phases

Diurnal amplitudes

Figure 7. Horizontal distribution of the diurnal phases in hours (**top**) and amplitudes in Kelvin (**bottom**) of the non-migrating tide component at 46 km for each longitude and latitude grid point.
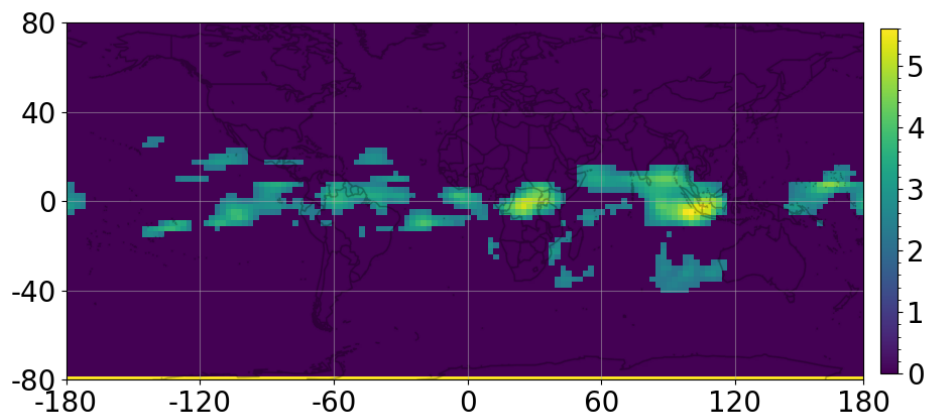

Figure 8. Horizontal distribution of the amplitude of the local tides after removing the non-migrating tides common to all longitudes (in Kelvin) of the non-migrating tide component at 46 km for each longitude and latitude grid point.
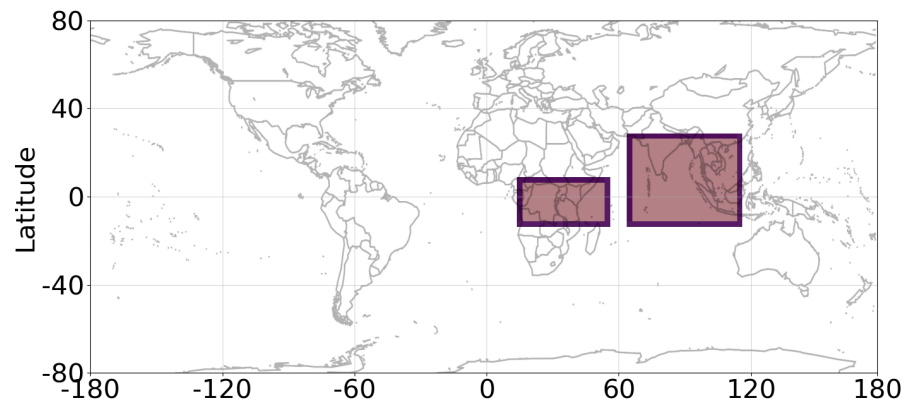
Figure 9. Geographic zones used to retrieve non-migrating tides. Zone IO is located around the Indian Ocean between 65 and 115° E in longitude and between 30° N and 10° S in latitude, and zone EA is centered over equatorial Africa between 15 and 55° E in longitude and between 10° N and 10° S in latitude.

Figure 10. Vertical profiles of amplitudes in temperature (**top**) and phases in hours (**bottom**) of the semi-diurnal (**left**) and diurnal (**right**) tides extracted from ERA5 meteorological analyses over the Indian Ocean (zone IO) in blue. Red dots are associated with another maximum in the histogram. Horizontal bars for the phase estimates correspond to the uncertainties.
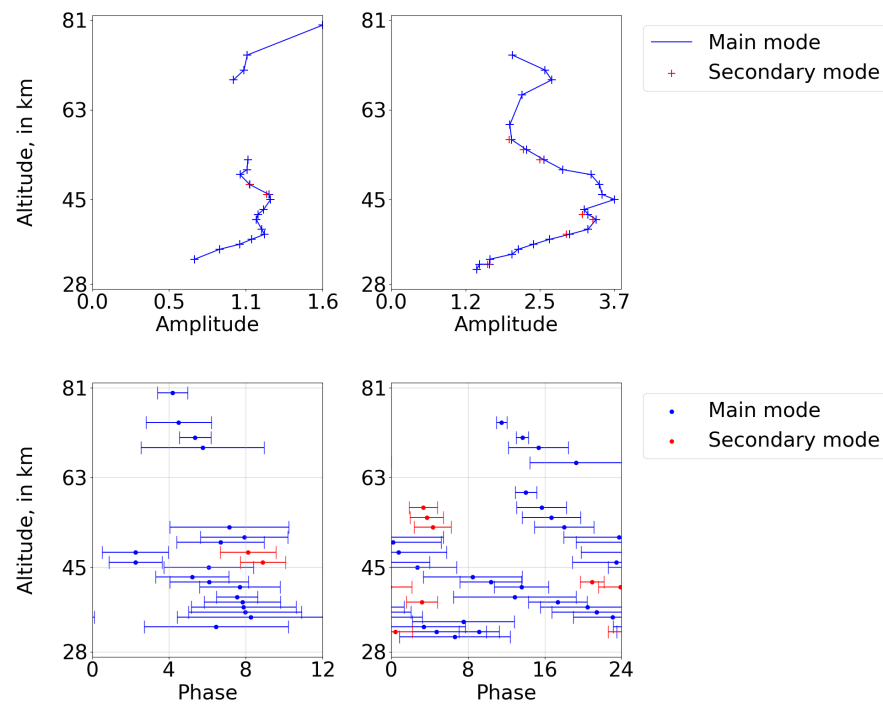
Figure 11. See caption for Figure 10, here applied to tropical Africa (zone TA).

6. Observation Requirements

This ERA5 analysis confirms that the model reproduces migrating tides with a reduced amplitude at mid-latitude. Over the tropics, diurnal changes associated with steady non-migrating tides over continents were identified. Their characteristics need to be further investigated in order to be validated on a global scale with observations. However, operational global wind and temperature observations are missing in the middle atmosphere. In locations where steady waves appear, it is necessary to sample air masses several times per day to be able to retrieve tides. Ground-based observations are useful for complementing space observations. The European ARISE network [38], including the NDACC network [39], maintains remote sensing measurements of the middle atmosphere, allowing for continuous measurements during a full diurnal cycle [6,8,9,21,23,40]. Some stations are located over the subtropics, allowing for local tidal retrieval. However, the network is not able to retrieve the largest non-migrating tides over the equator when no upper atmosphere observatories are deployed in these areas. In addition, while convective areas have a permanent roof made up of convective clouds, microwave technology [41] is preferred to lidar because the latter's abilities are highly insensitive to cloud cover. This is a critical issue because non-migrating tides are associated with atmospheric water vapor content, known to be challenging to accurately simulate in numerical weather/climate models.

A recent study has been performed to envision how to provide temperature measurements unbiased by solar migrating tides [22]. This study suggests the use of a constellation of nano-satellites in different sun-synchronous orbits to increase the number of measurements per day over a given location for a reasonable cost. One potential proposed method is based on molecular scattering observed by limb viewing. This method provides the best vertical resolution. It was first used to view bright limbs from space using the Solar Mesosphere Explorer [42]. A similar method was used in space experiments like WINDII on UARS [43], and more recently it was successfully tested through the GOMOS experiment [44]. In the future, time continuity will be ensured by the ALTIUS (Atmospheric Limb Tracker for Investigation of the Upcoming Stratosphere) payload [45]. However, all these experiments that exhibit a similar observational geometry were not initially planned to provide temperatures and instead are reasearch systems with a complex setup. However,

these observations of the bright limb can be performed with a much simpler system that can employ CubeSat technology [22]. In 1999, a collaboration between California Polytechnic State University and Stanford University, California, developed a small educational platform called CubeSat, which was designed for space exploration and research for academic purposes [46]. CubeSats are now a common form of small spacecraft that can weigh only a few kilograms (up to 30 kg) and that correspond to a standard based on a form factor of a 10 cm square cube called unit (U). This principle allows easy deployment in space and use of COTS (commercial off-the-shelf) considerably reducing the price of each individual satellite. Retrieval of migrating tides require at least five payloads simultaneously in space to separate diurnal and semi-diurnal components. The presence of non-migrating tides yields much more information and requires increasing the number of space platforms to increase the sampling of these specific areas if we want to derive the local tidal characteristics directly from observations alone. This strategy has already been deployed to investigate several other issues, such as the radiative balance of Earth [47,48].

7. Discussions and Conclusions

If migrating and non-migrating tides are correctly simulated in numerical weather and climate models, it means that both radiative and dynamic processes are correctly taken into account and can somehow validate models on hourly scales. The ERA5 model is currently one of the most sophisticated representations of our atmosphere for weather and climate forecasting. The analysis of the new data from the European center ERA5 allows us to develop a new methodology to separate migrating tides from non-migrating tides by an objective analysis of histograms by longitude where migrating tides by definition must have similar characteristics. It appears that the characteristics of the migrating modes are in fairly good agreement up to 60 km, even if the amplitudes at mid-latitudes remain twice as large compared to the simulations with the GSWM model, as already reported by previous studies. This is not surprising because daily comparisons with the observations showed that the variability in the upper part of the model was clearly damped and permanently close to the climatology [32,49]. Although non-migrating modes appear to exist at all latitudes in the model, the largest amplitudes appear around the equator where the water vapor content may be regionally very important due to convection. However, at the present time, no data are available to validate their characteristics. This study is a preliminary approach showing that migrating and non-migrating tidal components co-exist in the model. It is likely that more sophisticated statistical methods can be used to extract the global tidal modes and anomalies associated with non-migrating local effects.

Lack of knowledge of tidal characteristics is a problem in the middle atmosphere for monitoring issues, but also because tides induce spectrum aliasing effects and thus undesirable fluctuations occur during data assimilation processes, for example. The use of a satellite constellation could partially solve this weakness. Constellations are only feasible if several small satellites are deployed simultaneously at low cost. With the limb observations, it is possible to derive temperature profiles with a good vertical resolution (1–2 km). This technique can be developed within small satellites like CubeSat and can then be deployed through a large constellation that can provide several observations each day over a single location, allowing us to take into account tidal fluctuations. These data would provide global coverage with an improved sampling rate, which could be incorporated into meteorological models. This will be crucial for providing accurate mesospheric temperature information.

Space observations could be supplemented by specific continuous observations of the tides from the ground in convective regions to observe local non-migrating tides. Therefore, the microwave technique, which is not affected by clouds, allows us to provide continuous observations in convective regions. Ozone and water vapor profiles can be derived with microwave spectrometers [12] and, more recently, wind and temperature profiles have also been produced with similar methods [50]. This issue needs to be taken into account when building infrastructure dedicated to middle atmosphere observation networks. The

international NDACC network [39] has suggested the use of microwave spectrometers to monitor composition changes, and it is possible to derive diurnal changes due to photo-dissociation over some ground-based locations. More recently, instrumental developments performed within the European ARISE network [38] have extended observations to the wind parameters and thus atmospheric tides in dynamic parameters. Such international efforts to provide continuous observations of the middle atmosphere need to continue over more locations in conjunction with the setting of a space constellation. More local observations are required over the tropical band. More analyses will be performed with new additional data or in parallel through intensive campaigns dedicated to diurnal investigations like the ones organized a decade ago [51].

References

1. Chapman, S.; Lindzen, R. *Atmospheric Tides*; Springer: Dordrecht, The Netherlands, 1970; Volume 10, p. 106. [CrossRef]
2. Morel, B.; Keckhut, P.; Bencherif, H.; Hauchecorne, A.; Megie, G.; Baldy, S. Investigation of the tidal variations in a 3-D dynamics-chemistry-transport model of the middle atmosphere. *J. Atmos. Sol. Terr. Phys.* **2004**, *66*, 251–265. [CrossRef]
3. Manson, A.; Meek, C.; Hagan, M.; Hall, C.; Hocking, W.; MacDougall, J.; Franke, S.; Riggin, D.; Fritts, D.; Vincent, R.; et al. Seasonal variations of the semi-diurnal and diurnal tides in the MLT: Multi-year MF radar observations from 2 to 70° N, and the GSWM tidal model. *J. Atmos. Sol. Terr. Phys.* **1999**, *61*, 809–828. [CrossRef]
4. Baron, P.; Murtagh, D.; Eriksson, P.; Mendrok, J.; Ochiai, S.; Pérot, K.; Sagawa, H.; Suzuki, M. Simulation study for the Stratospheric Inferred Winds (SIW) sub-millimeter limb sounder. *Atmos. Meas. Tech.* **2018**, *11*, 4545–4566. [CrossRef]
5. Hocking, W.; Hocking, A. Temperature tides determined with meteor radar. *Ann. Geophys.* **2002**, *20*, 1447–1467. [CrossRef]
6. Leblanc, T.; McDermid, I.; Ortland, D. Lidar observations of the middle atmospheric thermal tides and comparison with the High Resolution Doppler Imager and Global Scale Wave Model: 2. October observations at Mauna Loa (19.5° N). *J. Geophys. Res. Atmos.* **1999**, *104*, 11931–11938. [CrossRef]
7. Chen, S.; Hu, Z.; White, M.; Chen, H.; Krueger, D.; She, C. Lidar observations of seasonal variation of diurnal mean temperature in the mesopause region over Fort Collins, Colorado (41° N, 105° W). *J. Geophys. Res. Atmos.* **2000**, *105*, 12371–12379. [CrossRef]
8. Kopp, M.; Gerding, M.; Hoffner, J.; Lubken, F.J. Tidal signatures in temperatures derived from daylight lidar soundings above Kuhlungsborn (54° N, 12° E). *J. Atmos. Sol. Terr. Phys.* **2015**, *127*, 37–50. [CrossRef]
9. Morel, B.; Bencherif, H.; Keckhut, P.; Baldy, S.; Hauchecorne, A. Evidence of tidal perturbations in the middle atmosphere over Southern Tropics as deduced from LIDAR data analyses. *J. Atmos. Sol. Terr. Phys.* **2002**, *64*, 1979–1988. [CrossRef]
10. She, C.; Li, T. Tidal perturbations and variability in the mesopause region over Fort Collins, Colorado (41° N, 105° W): Continuous multi-day temperature and wind lidar observations. *Geophy. Res. Lett.* **2004**, *31*, 24011. [CrossRef]
11. Ricaud, P.; Brillet, J.; De La Noe, J.; Parisot, J. Diurnal and seasonal variations of stratomesospheric ozone: Analysis of ground-based microwave measurements in Bordeaux, France. *J. Geophys. Res.* **1991**, *96*, 18617–18629. [CrossRef]
12. Haefele, A.; Hocke, K.; Kampfer, N.; Keckhut, P.; Marchand, M.; Bekki, S.; Morel, B.; Egorova, T.; Rozanov, E. Diurnal changes in middle atmospheric H20 and O3: Observations in the Alpine region and climate models. *J. Geophys. Res.* **2008**, *113*. [CrossRef]

13. Lieberman, R. Non-migrating diurnal tides in the equatorial middle atmosphere. *J. Atmos. Sci.* **1991**, *48*, 1112–1123. [CrossRef]
14. Wild, J.; Gelman, M.; Miller, A.; Chanin, M.L.; Hauchecorne, A.; Keckhut, P.; Farley, R.; Dao, P.; Gobbi, G.P.; Adriani, A.; et al. Comparison OF Stratospheric Temperature from several lidars using NMC and MLS data as transfer reference. *Geophys. Res. Lett.* **1995**, *100*, 11105–11111. [CrossRef]
15. Huang, F.; McPeters, R.; Bhartia, P.; Mayr, H.; Frith, S.; Russell, J., III; Mlynczak, M. Temperature diurnal variations (migrating tides) in the stratosphere and lower mesosphere based on measurements from SABER on TIMED. *J. Geophy. Res.* **2010**, *115*. [CrossRef]
16. Keckhut, P.; Gelman, M.; Wild, J.; Tissot, F.; Miller, A.; Hauchecorne, A.; Chanin, M.; Fishbein, E.; Gille, J.; Russell, J., III; et al. Semidiurnal and diurnal temperature tides (305 km): Climatology and effect on UARS-lidar data comparison. *J. Geophys. Res.* **1996**, *101*, 102990310. [CrossRef]
17. Thompson, D.; Seidel, D.; Randel, W.; Zou, C.Z.; Butler, A.; Mears, C.; Osso, A.; Long, C.; Lin, R. The mystery of recent stratospheric temperature trends. *Nature* **2012**, *491*, 692–697. [CrossRef]
18. Keckhut, P.; Funatsu, B.; Claud, C.; Hauchecorne, A. Tidal effects on stratospheric temperature series derived from successive Advanced Microwave Sounding Units. *Q. J. R. Meteorol. Soc.* **2015**, *141*, 477–483. [CrossRef]
19. Hagan, M.; Forbes, J.M.; Vial, F. On modeling migrating solar tides. *Geophys. Res. Lett.* **1995**, *22*, 893–896. [CrossRef]
20. Hagan, M. GSWM-98: Results for migrating solar tides. *J. Geophys. Res. Space Phys.* **1999**, *104*, 6813–6827. [CrossRef]
21. Raju, U.J.P.; Keckhut, P.; Courcoux, Y.; Marchand, M.; Bekki, S.; Morel, B.; Bencherif, H.; Hauchecorne, A. Nocturnal temperature changes over tropics during CAWSES-III campaign: Comparison with numerical models and satellite data. *J. Atmos. Sol. Terr. Phys.* **2010**, *72*, 1171–1179. [CrossRef]
22. Keckhut, P.; Hauchecorne, A.; Meftah, M.; Khaykin, S.; Claud, C.; Simoneau, P. Middle-Atmosphere Temperature Monitoring Addressed with a Constellation of CubeSats Dedicated to Climate Issues. *J. Atmos. Ocean. Technol.* **2021**, *38*, 685–693. [CrossRef]
23. Baumgarten, K.; Stober, G. On the evaluation of the phase relation between temperature and wind tides based on ground-based measurements and reanalysis data in the middle atmosphere. *Ann. Geophys.* **2019**, *37*, 581–602. [CrossRef]
24. Khaykin, S.M.; Pommereau, J.P.; Hauchecorne, A. Impact of land convection on temperature diurnal variation in the tropical lower stratosphere inferred from COSMIC GPS radio occultations. *Atmos. Chem. Phys.* **2013**, *13*, 6391–6402. [CrossRef]
25. Harper, K.; Uccellini, L.W.; Kalnay, E.; Carey, K.; Morone, L. 50th Anniversary of Operational Numerical Weather Prediction. *Bull. Am. Meteorol. Soc.* **2007**, *88*, 639–650. [CrossRef]
26. Holton, J.R. *An Introduction to Dynamic Meteorology*; International Geophysics; Academic Press: Cambridge, MA, USA, 2004; Volume 88, pp. 11–12. . [CrossRef]
27. Lorenc, A. Atmospheric modelling, data assimilation and predictability. By Eugenia Kalnay. Cambridge University Press. 2003. pp. xxii + 341. ISBNs 0 521 79179 0, 0 521 79629 6. *Q. J. R. Meteorol. Soc.* **2003**, *129*. [CrossRef]
28. Hersbach, H.; Bell, B.; Berrisford, P.; Hirahara, S.; Horányi, A.; Muñoz-Sabater, J.; Nicolas, J.; Peubey, C.; Radu, R.; Schepers, D.; et al. The ERA5 global reanalysis. *Q. J. R. Meteorol. Soc.* **2020**, *146*, 1999–2049. [CrossRef]
29. Lastovika, J. Forcing of the ionosphere by waves from below. *J. Atmos. Sol. Terr. Phys.* **2006**, *68*, 479–497. [CrossRef]
30. Parzen, E. On Estimation of a Probability Density Function and Mode. *Ann. Math. Stat.* **1962**, *33*, 1065–1076. [CrossRef]
31. Pedregosa, F.; Varoquaux, G.; Gramfort, A.; Michel, V.; Thirion, B.; Grisel, O.; Blondel, M.; Prettenhofer, P.; Weiss, R.; Dubourg, V.; et al. Scikit-learn: Machine Learning in Python. *J. Mach. Learn. Res.* **2011**, *12*, 2825–2830.
32. Mariaccia, A.; Keckhut, P.; Hauchecorne, A.; Claud, C.; Le Pichon, A.; Meftah, M.; Khaykin, S. Assessment of ERA-5 Temperature Variability in the Middle Atmosphere Using Rayleigh LiDAR Measurements between 2005 and 2020. *Atmosphere* **2022**, *13*, 242. [CrossRef]
33. Held, I.M.; Soden, B.J. Water Vapor Feedback and Global Warming. *Ann. Rev. Energy Environ.* **2000**, *25*, 441–475. [CrossRef]
34. Woolnough, S.J.; Slingo, J.M.; Hoskins, B.J. The Diurnal Cycle of Convection and Atmospheric Tides in an Aquaplanet GCM. *J. Atmos. Sci.* **2004**, *61*, 2559–2573. [CrossRef]
35. Roca, R.; Bergers, J.C.; Brogniez, H.; Capderou, M.; Chambon, P.; Chomette, O.; Cloche, S.; Fiolleau, T.; Jobard, I.; Lemond, J.; et al. On the water and energy cycles in the Tropics. *C. R. Geosci.* **2010**, *342*, 390–402. [CrossRef]
36. Alexander, S.P.; Tsuda, T. Observations of the diurnal tide during seven intensive radiosonde campaigns in Australia and Indonesia. *J. Geophys. Res. Atmos.* **2008**, *113*, 581–602. [CrossRef]
37. Liu, X.M.; Riviere, E.D.; Marecal, V.; Durry, G.; Hamdouni, A.; Arteta, J.; Khaykin, S. Stratospheric water vapour budget and convective overshooting the tropopause: Modelling study from SCOUT-AMMA. *Atmos. Chem. Phys.* **2010**, *10*, 8267–8286. [CrossRef]
38. Blanc, E.; Ceranna, L.; Hauchecorne, A.; Charlton-Perez, A.; Marchetti, E.; Evers, L.; Kvaerna, T.; Lastovicka, J.; Eliasson, L.; Crosby, N.; et al. Toward an Improved Representation of Middle Atmospheric Dynamics Thanks to the ARISE Project. *Surv. Geophys.* **2017**. [CrossRef]
39. Kurylo, M. Network for the detection of stratospheric change (NDSC). *Remote Sens. Atmos. Chem.* **1991**, *1491*, 168–174.
40. Hagen, J.; Hocke, K.; Stober, G.; Pfreundschuh, S.; Murk, A.; Kampfer, N. First measurements of tides in the stratosphere and lower mesosphere by ground-based Doppler microwave wind radiometry. *Atmos. Chem. Phys.* **2020**, *20*, 2367–2386. [CrossRef]
41. Stähli, O.; Murk, A.; Kämpfer, N.; Mätzler, C.; Eriksson, P. Microwave radiometer to retrieve temperature profiles from the surface to the stratopause. *Atmos. Meas. Tech.* **2013**, *6*, 2477–2494. [CrossRef]

42. Clancy, R.; Rusch, D.; Callan, M. Temperature minima in the average thermal structure of the middle mesosphere (70–80 km) from analysis of 40- to 92-km SME global temperature profiles. *J. Geophys. Res.* **1994**, *99*, 19001–19020. [CrossRef]

43. Shepherd, M.; Reid, B.; Zhang, S.; Solheim, B.; Shepherd, G.; Wickwar, V.; Herron, J. Retrieval and validation of mesospheric temperatures from Wind Imaging Interferometer observations. *J. Geophys. Res.* **2001**, *106*, 24813–24830. [CrossRef]

44. Hauchecorne, A.; Blanot, L.; Wing, R.; Keckhut, P.; Khaykin, S.; Bertaux, J.L.; Meftah, M.; Claud, C.; Sofieva, V. A new MesosphEO data set of temperature profiles from 35 to 85 km using Rayleigh scattering at limb from GOMOS/ENVISAT daytime observations. *Atmos. Meas. Tech.* **2019**, *12*, 749–761. [CrossRef]

45. Fussen, D.; Baker, N.; Debosscher, J.; Dekemper, E.; Demoulin, P.; Errera, Q.; Franssens, G.; Mateshvili, N.; Pereira, N.; Pieroux, D.; et al. The ALTIUS atmospheric limb sounder. *J. Quant. Spectrosc. Radiat. Transf.* **2019**, *238*, 106542. [CrossRef]

46. Yost, B. *State-of-the-Art Small Spacecraft Technology*; Weston, S., Ed.; NASA Center for AeroSpace Information, Hanover, MD, USA; Ames Research Center: Hanover, MD, USA; NASA: San Jose, CA, USA, 2021; Volume NASA.

47. Meftah, M.; Damé, L.; Keckhut, P.; Bekki, S.; Sarkissian, A.; Hauchecorne, A.; Bertran, E.; Carta, J.P.; Rogers, D.; Abbaki, S.; et al. UVSQ-Sat, a Pathfinder CubeSat Mission for Observing Essential Climate Variables. *Remote Sens.* **2020**, *12*, 92. [CrossRef]

48. Meftah, M.; Boust, F.; Keckhut, P.; Sarkissian, A.; Boutéraon, T.; Bekki, S.; Damé, L.; Galopeau, P.; Hauchecorne, A.; Dufour, C.; et al. INSPIRE-SAT 7, a Second CubeSat to Measure the Earth's Energy Budget and to Probe the Ionosphere. *Remote Sens.* **2022**, *14*, 186. [CrossRef]

49. Le Pichon, A.; Assink, J.; Heinrich, P.; Blanc, E.; Charlton-Perez, A.; Lee, C.; Keckhut, P.; Hauchecorne, A.; Rafenacht, R.; Kampfer, N.; et al. Comparison of co-located independent ground-based middle-atmospheric wind and temperature measurements with Numerical Weather Prediction models. *J. Geophys. Res. Atmos.* **2015**, *120*, 8318–8331. [CrossRef]

50. Rüfenacht, R.; Kämpfer, N.; Murk, A. First middle-atmospheric zonal wind profile measurements with a new ground-based microwave Doppler-spectro-radiometer. *Atmos. Meas. Tech.* **2012**, *5*, 2647–2659. [CrossRef]

51. Ward, W.E.; Oberheide, J.; Goncharenko, L.P.; Nakamura, T.; Hoffmann, P.; Singer, W.; Chang, L.C.; Du, J.; Wang, D.Y.; Batista, P.; et al. On the consistency of model, ground-based, and satellite observations of tidal signatures: Initial results from the CAWSES tidal campaigns. *J. Geophys. Res. Atmos.* **2010**, *115*. [CrossRef]